



Experimental electronic structure of In_2O_3 and Ga_2O_3

To cite this article: Christoph Janowitz *et al* 2011 *New J. Phys.* **13** 085014

View the [article online](#) for updates and enhancements.

Related content

- [The surface band structure of \$\text{-Ga}_2\text{O}_3\$](#)
- [Resonant Photoemission at the \$\text{O}1s\$ threshold to characterize \$\text{-Ga}_2\text{O}_3\$ single crystals](#)
- [Polaron character of the near- \$E_F\$ band of cleaved \$\text{In}_2\text{O}_3\(111\)\$ single crystals](#)

Recent citations

- [Dislocation classification of a large-area \$\text{-Ga}_2\text{O}_3\$ single crystal via contrast analysis of affine-transformed X-ray topographs](#)
Yongzhao Yao *et al*
- [Structural, electronic, elastic, power, and transport properties of \$\text{Ga}_2\text{O}_3\$ from first principles](#)
Samuel Poncé and and Feliciano Giustino
- [Identification of Burgers vectors of dislocations in monoclinic \$\text{-Ga}_2\text{O}_3\$ via synchrotron x-ray topography](#)
Yongzhao Yao *et al*

Experimental electronic structure of In_2O_3 and Ga_2O_3

Christoph Janowitz^{1,3,5}, Valentina Scherer¹,
Mansour Mohamed¹, Alica Krapf¹, Helmut Dwelk¹,
Recardo Manzke¹, Zbigniew Galazka², Reinhard Uecker²,
Klaus Irmscher², Roberto Fornari², Marcel Michling³,
Dieter Schmeißer³, Justin R Weber⁴, Joel B Varley⁴
and Chris G Van de Walle⁴

¹ Humboldt-Universität zu Berlin, Institut für Physik, Newtonstr. 15,
D-12489 Berlin, Germany

² Leibniz-Institut für Kristallzüchtung, Max-Born-Strße, 2 D-12489 Berlin,
Germany

³ Brandenburgische Technische Universität, K-Wachsmann-Allee 1,
D-03046 Cottbus, Germany

⁴ Materials Department, University of California, Santa Barbara,
CA 93106-5050, USA

E-mail: janowitz@physik.hu-berlin.de

New Journal of Physics **13** (2011) 085014 (14pp)

Received 4 April 2011

Published 16 August 2011

Online at <http://www.njp.org/>

doi:10.1088/1367-2630/13/8/085014

Abstract. Transparent conducting oxides (TCOs) pose a number of serious challenges. In addition to the pursuit of high-quality single crystals and thin films, their application has to be preceded by a thorough understanding of their peculiar electronic structure. It is of fundamental interest to understand why these materials, transparent up to the UV spectral regime, behave also as conductors. Here we investigate In_2O_3 and Ga_2O_3 , two binary oxides, which show the smallest and largest optical gaps among conventional n -type TCOs. The investigations on the electronic structure were performed on high-quality n -type single crystals showing carrier densities of $\sim 10^{19} \text{ cm}^{-3}$ (In_2O_3) and $\sim 10^{17} \text{ cm}^{-3}$ (Ga_2O_3). The subjects addressed for both materials are: the determination of the band structure along high-symmetry directions and fundamental gaps by angular resolved photoemission (ARPES). We also address the orbital character of the valence- and conduction-band regions by exploiting photoemission cross

⁵ Author to whom any corresponding should be addressed.

sections in x-ray photoemission (XPS) and by x-ray absorption (XAS). The observations are discussed with reference to calculations of the electronic structure and the experimental results on thin films.

Contents

1. Introduction	2
2. Experimental details	2
3. In₂O₃: results and discussion	4
4. Ga₂O₃: results and discussion	11
5. Conclusions	13
Acknowledgments	13
References	14

1. Introduction

Despite the vast and quickly growing number of applications of transparent conducting oxides (TCOs), their electronic structure still poses a number of fundamental open questions. Among them are the size and character of the band gap [1], details of the band structure [2] and the possible existence of a charge accumulation layer on the surface, as observed on films of In₂O₃ [3]. Since TCOs are materials that may have either conducting or semiconducting properties, these questions are also interesting from the standpoint of basic research. To date, the largest number of studies has been performed on ZnO, a prominent member of the TCO family, which has the advantage that bulk single crystals can be grown from the melt by the Bridgman method [4]. Other TCOs such as In₂O₃ and Ga₂O₃, which are the subject of this paper are more difficult to grow in the form of large single crystals. Bulk Ga₂O₃ single crystals that are a subject of this paper were scarcely available in the past. In recent years, the Czochralski method [5] has been successfully applied to the growth of bulk Ga₂O₃ crystals from the melt. For this reason, previous spectroscopic studies of In₂O₃ and Ga₂O₃ used thin films grown by lower-quality methods. We will address the issues mentioned above regarding high-quality single crystals, whose surface was cleaved *in situ* under ultrahigh vacuum (UHV). This allows us to access the true three-dimensional (3D) electronic structure of unstrained material without any residual contamination due to an evaporation process. In this paper, we study the band structure of Ga₂O₃ and In₂O₃ single crystals by angular resolved photoemission (ARPES) and determine the size and character of the fundamental band gap, thus addressing the controversial issue of the magnitude of the band gap as determined by optical methods. Comparisons with first-principles calculations further elucidate the issue. Finally, the orbital character of the filled density of states (DOS) is determined by x-ray photoemission at different energies by exploiting calculated photoionization cross sections. For the unfilled DOS, we use information from x-ray absorption at different absorption edges.

2. Experimental details

Experiments were performed at Helmholtz-Zentrum Berlin (HZB) (formerly BESSY), Berlin, on two beamlines. High-resolution photoemission was performed on both TCOs at room

temperature on the 5 m normal incidence monochromator of the beamline BEST with an SES2002 analyzer by utilizing the radiation of BESSY II in the photon energy range of 15–39 eV. The radiation impinged at an angle of 90° on the electron analyzer in the plane of the axis of the electron lens. The angular scans were performed by rotating the sample under this fixed in and out geometry. An energy resolution of 20 meV and an angle resolution of 0.1° were found to be sufficient to resolve the essential details. For In_2O_3 and Ga_2O_3 , preparation of the (111) and the (100), plane, respectively, was done by cleavage *in situ*, unlike in previous studies using evaporated films or annealing under vacuum [2]. Ga_2O_3 -cleavage planes were also characterized prior to measurements by surface techniques such as low-energy diffraction (LEED) and scanning tunneling spectroscopy (STM). The STM pictures showed no surface imperfections on the scale down to nanometer resolution. The stoichiometry of In_2O_3 and Ga_2O_3 was checked by energy-dispersive x-ray spectroscopy (EDX). X-ray diffraction was used to determine the crystal structure and lattice parameters. The carrier concentration, resistivity and mobility of In_2O_3 were determined by the four- and five-point contact method and the Hall effect. Typical values at 300 K of $n = 1.3 \times 10^{19} \text{ cm}^{-3}$, $\rho = 8.5 \times 10^{-3} \Omega \text{ cm}$ and $\mu = 66 \text{ cm}^2 \text{ V}^{-1} \text{ s}^{-1}$ were obtained for In_2O_3 . Van der Pauw measurements on Ga_2O_3 yielded values of $n \sim 5.0 \times 10^{17} - 6.0 \times 10^{17} \text{ cm}^{-3}$, $\rho \sim 0.1 - 0.2 \Omega \text{ cm}$ and $\mu \sim 110 - 130 \text{ cm}^2 \text{ V}^{-1} \text{ s}^{-1}$.

Sample orientation was obtained from Laue diffraction. Point contacts of molten tin were fabricated on the back of Ga_2O_3 -crystals by high voltage, yielding good ohmic contacts of 3Ω between such points on one surface and $1.5 \text{ k}\Omega$ between contacts on the opposite sides of the crystal. Possible charging was checked by applying different photon intensities in the photoemission. Absolutely no shift of the spectra was observed, thereby excluding any charging of the sample. It was found sufficient to contact the In_2O_3 crystals using only tempered silver epoxy glue. High-quality β - Ga_2O_3 single crystals, grown by the Czochralski method in the Institut für Kristallzüchtung (IKZ), were used [5]. The In_2O_3 crystals were grown by chemical vapor transport at the Humboldt University.

For the XPS and XAS measurements, synchrotron light was incident on the PGM monochromator of the U49/2 beam line and focused on the cleaved single-crystal sample in a 45° incidence geometry [6]. The emitted electrons were collected in the angle-integrated mode with an 180° hemispherical energy analyzer, Specs Phoibos 150, positioned at an emission angle of 45° . The total energy resolution was about 150 meV for 640 eV excitation energy and 200 meV for 1000 eV excitation energy. The photon energy range of the U49/2 beam line in BESSY II is very large, covering energies as low as 90 up to 1800 eV (www.bessy.de). We have chosen a photon energy of 640 eV for the surface-sensitive investigation of the In3d and O1s core level peaks. Setting the emission angle at 45° further increased the surface sensitivity. By choosing the photon energy of 1000 eV we were able to investigate the In3d and O1s core levels also in the bulk. Thanks to these settings, we can show here very sensitive measurements that are not possible with standard laboratory sources. The XAS spectra were recorded using total electron yield (TEY) by measuring the drift current on the sample. The raw spectra were divided by the incoming photon flux and then a Shirley background was subtracted.

Figure 1 shows the local structure of In_2O_3 . It has a total of 80 atoms per unit cell, not all of which are depicted. The structure is body-centered cubic (Bixbyite) and has the space group Ia $\bar{3}$.

The lattice constant is $a = 10.117 \text{ \AA}$. In the bixbyite structure, indium atoms occupy two symmetrically inequivalent sites denoted by their Wyckoff position. The In-b-site is at the body diagonal of the two oxygen vacancies in the upper right cube. For the In-b-site the coordination

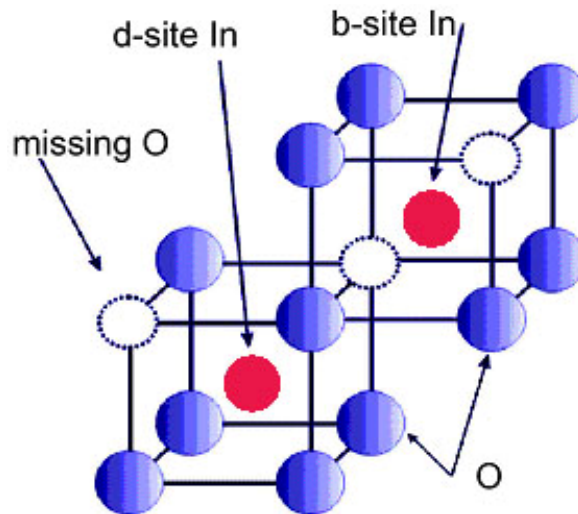


Figure 1. Local structure of In_2O_3 . Open circles denote oxygen vacancies, blue spheres oxygen atoms and red spheres indium atoms. A quarter of the anions are missing in the ideal structure, arranged at either a face diagonal (lower left) or a body diagonal (upper right). There are 48 anions in edge positions, 16 missing anions, 8 cations in b-positions and 24 cations in d-positions, resulting in a total of 80 atoms per unit cell.

number is $Z = 6$ oxygen atoms, which are all in equidistant positions. The In-d-site, shown in the cube on the lower left, has two oxygen vacancies at the face diagonal. The In-d-site also has $Z = 6$ but three different O-distances.

The unit cell of Ga_2O_3 is depicted in figure 2. Ga_2O_3 crystallizes in the base-centered monoclinic structure (space group $C2/m$) with lattice parameters $a = 12.214(3) \text{ \AA}$, $b = 3.0371(9) \text{ \AA}$, $c = 5.7981(9) \text{ \AA}$, $\beta = 103.83^\circ$ and four Ga_2O_3 formula units per 20-atom unit cell [7].

3. In_2O_3 : results and discussion

In figure 3, we show ARPES spectra taken along the surface normal, i.e. along the ΓP direction of the Brillouin zone (BZ), which is also included for reference. Both the valence band (VB) and the bottom of the conduction band are detected, the latter as a weak emission (see the figure caption). Due to the large number of 80 atoms per unit cell, one cannot expect to resolve all individual bands resulting from this huge unit cell. Instead, a strong, upward dispersing structure, consisting of two substructures, forms between photon energies of 15 and -25 eV . The center of gravity of the two substructures has its minimum binding energy at a photon energy of 18 eV, as denoted by the red curve and the arrow in figure 3. In figure 3, the intensity plot of the ‘band gap’ region clearly shows the upward dispersion of the topmost VB state towards the Γ -point and also the appearance of emission due to the CBM at the Γ -point. The issue of the topmost valence-band state will also be treated in the following text and in figure 4. It is not instructive to plot the band structure, since not all details (bands) for comparison with theory are resolvable. However, due to the strong dispersion perpendicular to the surface for both the VB

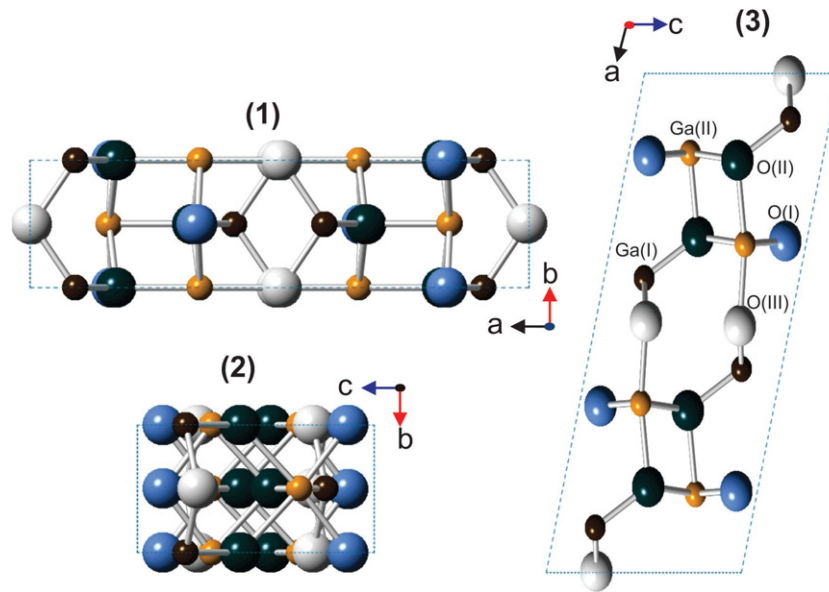


Figure 2. Unit cell of Ga_2O_3 . It possesses two inequivalent Ga sites: Ga(I), Ga(II) and three inequivalent O-sites: O(I), O(II) and O(III). The Ga(I) sites have tetrahedral coordination, and the Ga(II) sites have octahedral coordination [9]. Depicted is the projection of the unit cell of $\beta\text{-Ga}_2\text{O}_3$ along the c-(1), a-(2) and b-axis (3).

states, the topmost valence-band state and the state formed from the bottom of the conduction band, one has strong arguments for an interpretation in terms of true three-dimensional (3D) bulk states. An interpretation in terms of surface states or two-dimensional states is less plausible. The weak emission at the Fermi energy is only observable at photon energies corresponding to the Γ -point, i.e. about 18 eV, and vanishes otherwise, again strengthening the interpretation of the signal as corresponding to electrons in the bulk conduction-band minimum (CBM). In studies of evaporated films, this photon-energy dependence was not reported; only the fact that the weak emission at the Fermi energy scaled with the doping level was reported [1, 3]. We ascribe this to a reduced three-dimensionality of thin-film samples. Given the high carrier concentration of our In_2O_3 samples, one can infer that a degenerate semiconductor is observed. Low-temperature measurements at different doping levels are necessary to further validate this conclusion. In future studies it may be possible to enhance the bulk sensitivity also by using very high or very low photon energies.

Since the CBM becomes observable in our spectra of In_2O_3 , it is possible to determine the absolute size of the band gap solely on the basis of ARPES data. In figure 4, the spectrum of the upper VB and that due to the small part of the conduction band below the Fermi energy are depicted. Both are taken at the bulk BZ center Γ . Since resolving individual bands at room temperature is not possible for the large bixbyite unit cell, we fitted the groups of bands by a procedure from the IGOR program (<http://www.wavemetrics.com>). A tentative fit described in the figure caption delivered a total of five peaks. The uppermost two are peak 2 at -3.6 eV and peak 3 at -4.2 eV. Taking the low binding energy onset of peak 2, respectively the emission appearing around -3 eV binding energy at a low temperature (30 K; see figure 4(d)), as the VB maximum (VBM) and the maximum of peak 1 as the CBM, one arrives at a lowest band gap

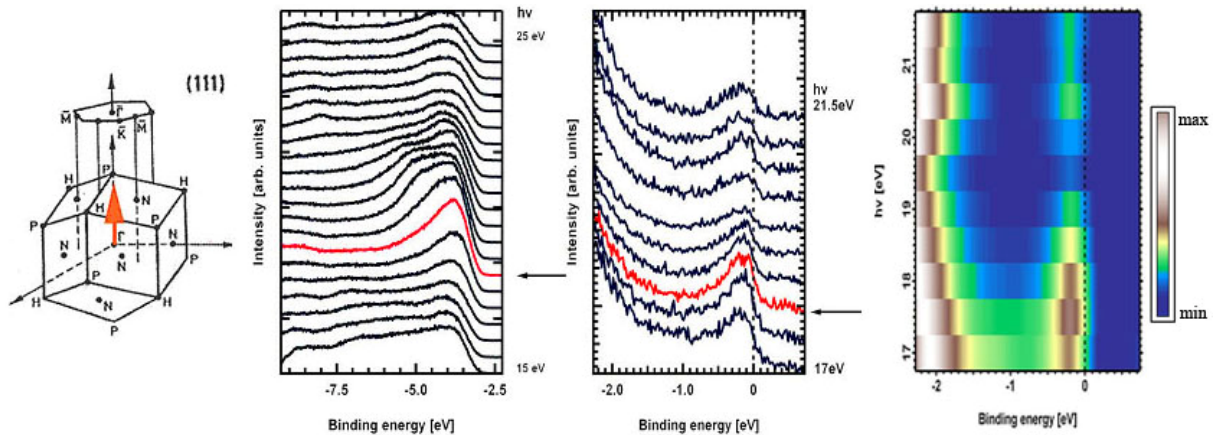


Figure 3. Left: BZ of In_2O_3 . Center left: ARPES spectra in normal emission of the VB region. The photon energy increases in steps of 0.5 eV from 15 to 33 eV. Center right: EDCs of the energy region around the Fermi energy on an expanded scale. One clearly sees here the appearance of the conduction band below the Fermi energy as a weak emission. The spectra corresponding to the VBM and CBM at the Γ -point are drawn in red and marked by an arrow. Right: intensity plot of the energy region around the Fermi energy on an expanded scale. The upward dispersion of the topmost VB state towards the Γ -point and the appearance of the emission due to the CBM at the Γ -point are clearly observed.

value of $E_{g1} = 2.63$ eV. The distance from peak 3 to peak 1 is $E_{g2} = 3.71$ eV. These values can be discussed in relation to optical data. Although ARPES and optical absorption are governed by similar dipole matrix elements, some transitions are not completely suppressed in ARPES measurements. Specifically, for a mixed polarization geometry with respect to the mirror planes, a free-electron final state always allows a transition, so that in practice no emissions in ARPES are suppressed completely. In optical measurements, the final states have a definite orbital character, which can lead to complete suppression of the transition due to dipole selection rules. Optical gaps of 2.63 and 3.72 eV measured on thin films were first reported by Weiher and Ley [9], where the weak feature at 2.63 eV was ascribed to an indirect transition. In a recent publication, it was shown that the VBM–CBM transition between states of $(T_g)\Gamma_4$ and $(A_g)\Gamma_1$ symmetry is forbidden by parity [1]. The first allowed transition between deeper VB states of $(T_u)\Gamma_8$ symmetry 0.8 eV below the VBM and CBM ($(A_g)\Gamma_1$) occurs at 3.7 eV. This last value fits nicely to our experimental ARPES value of 3.71 eV. When scanning the directions perpendicular to normal emission (k_{\parallel}) in all the symmetry directions, the bands disperse to a higher binding energy. The VBM is therefore located at the Γ -point, i.e. the band gap is direct.

The transparency in the visible range of the electromagnetic spectrum is due to optical forbidden transitions.

Since no individual bands can be resolved it is instructive to compare experimental and theoretical information on the orbital character of the filled and unfilled states. The top panel of figure 5 shows the theoretical projected density of states (PDOS) of Karazhanov *et al* [10], which shows three distinct VB regions discussed in the figure caption. Similar results were published by Fuchs and Bechstedt [11]. The three overview scans of the full VB region, which include the semicore In 4d states, can also be separated into three groups (see the figure caption). While

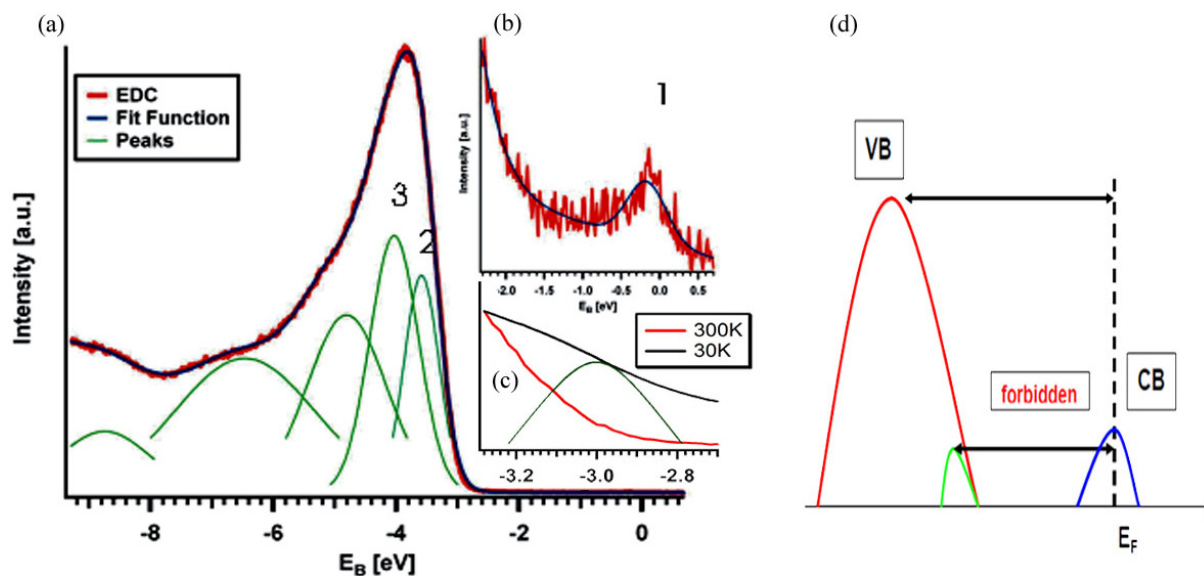


Figure 4. ARPES spectra of In₂O₃ at 18 eV photon energy. (a) Global fit to the valence bands 2 and 3 denote peaks due to valence states as obtained by fitting with ‘Multipeak Fitting’ from the IGOR program (<http://www.wavemetrics.com>). A total of five valence states were proposed by the program. (b) Fit to the region near the Fermi level. 1 denotes the peak due to the bottom of the conduction band, just dispersing slightly below the Fermi energy. (c) Detail of the upper VB region at 300 and 30 K. At low temperature, increasing intensity at about 3 eV binding energy is observed and can be interpreted as due to the topmost valence band. (d) Schematic drawing of the states involved in the optical transitions: red due to states 3 and 2 of figure 4(a), green due the upper VB state of figure 4(c) and blue due to the conduction-band state of figure 4(b). This assignment is in line with the calculations of Walsh [1], who showed that transitions from the upper VB states are forbidden by symmetry.

the energy positions of regions I and III correspond well with theory, the experimental value of region II is roughly 2 eV lower in binding energy. Also from an inspection of photoionization cross sections [12], only the strong In 4d character of region I and the In 5s, In 5p and In 4d character of region III are confirmed. Region II, theoretically claimed to be of In 4d character as in region I, should also increase its relative intensity at higher photon energies. Instead it vanishes. Further calculations may resolve the character of this state II.

In the combined picture of figure 6 we show the DOS of the VB and the PDOS of the conduction band, both referenced to the Fermi energy E_F . The Fermi-energy level for the XAS data was calculated by subtracting the binding energy of the O 1s core level from the excitation energy. The Fermi energy for the XPS is known from a calibration with a gold sample. From the XAS spectra one can state that the CBM is composed mainly of O with some In contributions. Applying symmetry selection rules with the O 1s and In 3d as initial states, one can conclude that we see mainly the O 2p character at lower binding energy and In 5p character at higher binding energy. The conduction band ends in, as also observed in ARPES, a weak feature at the Fermi energy.

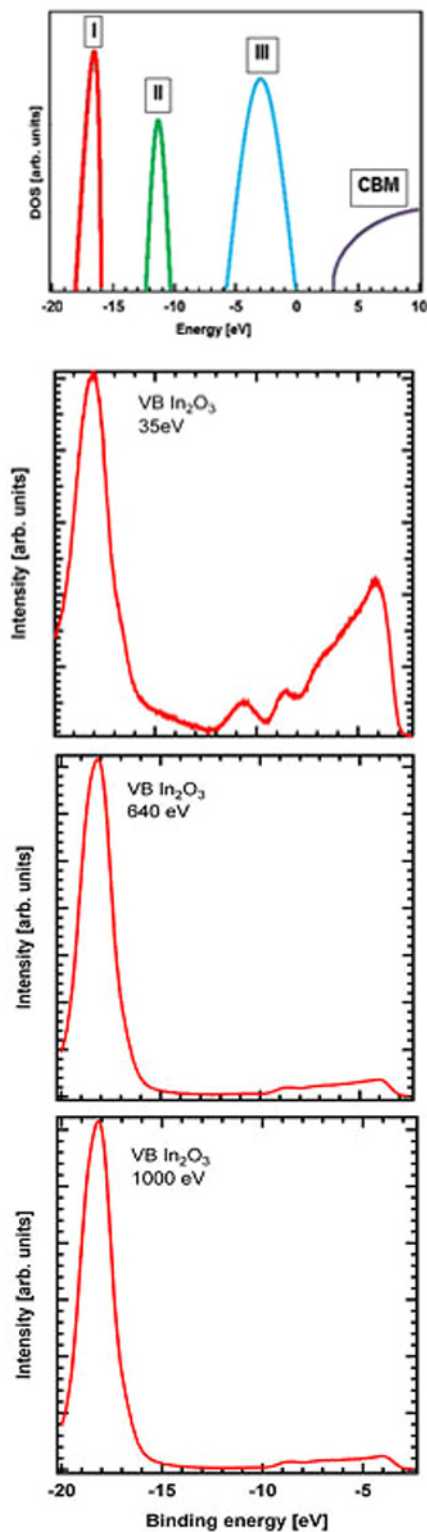


Figure 5. From top to bottom: Density of states (DOS) due to Karazhanov *et al* [11]. The energy axis is referenced to the VBM. Note that this differs from the reference in our experimental curves, where the Fermi energy corresponds to zero. The VB DOS is grouped into three separate regions. Region I around 17 eV

Figure 5. (Continued.) below the VBM is mainly composed of In 4d and O 2s states, region II at 12 eV below the VBM is almost purely In 4d and region III from 0 to -6 eV below VBM should be composed of In 5s,p and In 4d and O 2p. The CBM is mainly of In 5s and O 2p character. Below are XPS spectra taken at 35 eV, 640 eV and 1000 eV photon energy. Here the binding energy is referenced to the experimentally determined Fermi energy. All three separate regions I, II, III experimentally observed at binding energies of -18 eV, -10.5 eV and between -3 eV and -9 eV are most clearly observable in the first spectrum taken at a photon energy of 35 eV. At higher excitation energy, the intensity of region II vanishes, while that of region I increases and that of region III decreases.

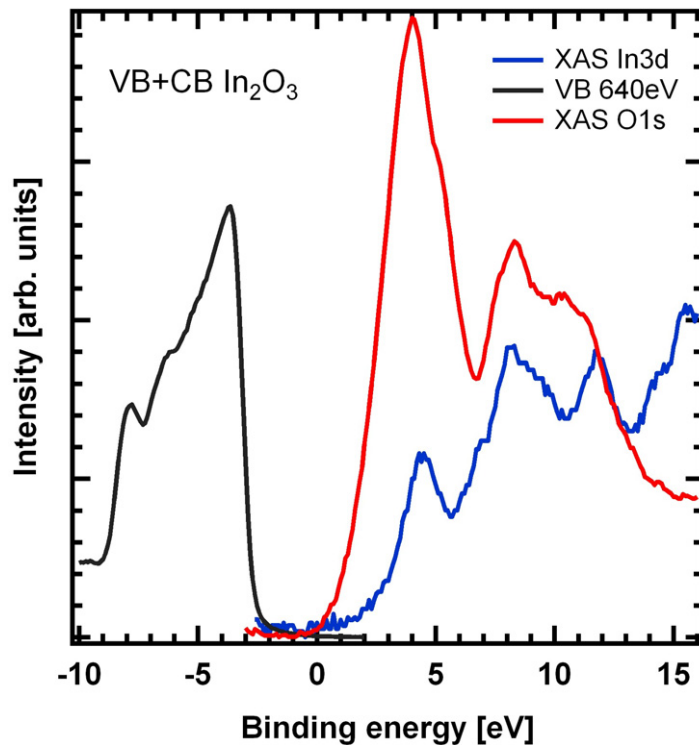


Figure 6. VB DOS obtained with XPS at 640 eV brought to a common energy scale with the projected density of unfilled states obtained by XAS on the O 1s and In 3d thresholds, respectively. The scaling to a common energy axis is described in the text. Since the In 3d core levels are split due to spin-orbit interaction by 9 eV, the In 3d XAS is repeating 9 eV above the Fermi-energy position; the crucial information is therefore in the first 9 eV above the Fermi energy.

Core-level spectra of the O 1s and the In 3d states are depicted in figure 7. One observes in both cases a split-off emission at higher binding energy. In the case of O, these are labeled O_I and O_{II} . The energy separation for the O shoulder is 1.6 eV and that of the In 3d shoulders

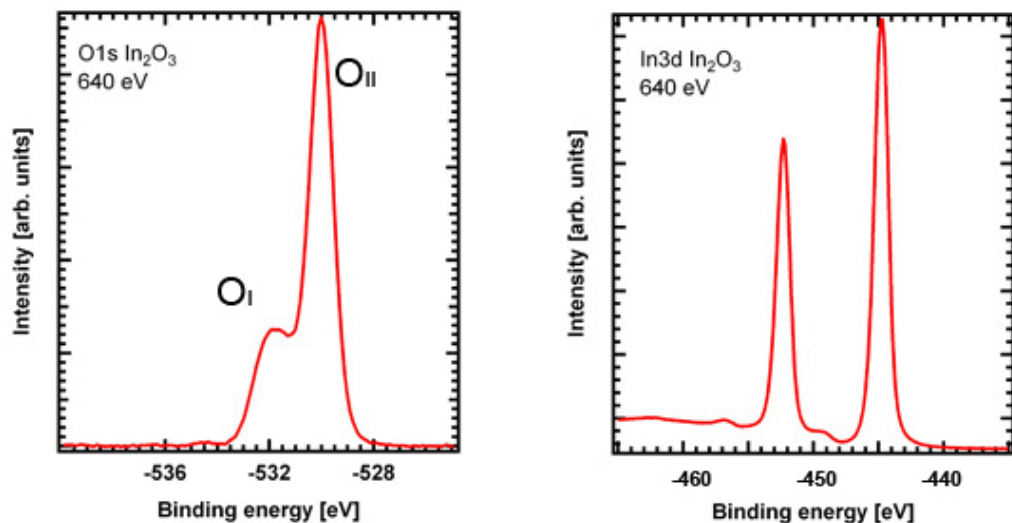


Figure 7. Oxygen 1s (left) and In $3d_{3/2}$ and In $3d_{5/2}$ core levels (right) observed at a photon energy of 640 eV. A strong shoulder labeled O_I is clearly seen in the main oxygen line labeled O_{II} . Also the In 3d core levels show a weaker shoulder. For details, see the text.

is 4.5 eV. The intensity ratio O_I/O_{II} is 1 : 3 at the photon energy of 640 eV and decreases for a higher photon energy of 1000 eV to 1 : 6 (not shown). At 1000 eV the In 3d shoulders are also decreased by this value.

One has to check whether the split excitations are due to different coordinated atoms in the ideal crystal structure. Since all 48 anions in edge positions are equivalent, this cannot be the reason for the observed O 1s splitting. The In occurs in In(d) and In(b) positions at a ratio of $24 : 8 = 3$, which is too high to match the experimentally found weak shoulder, which gets even weaker at higher photon energy.

Fan and Goodenough [13] were the first to investigate Sn-doped In_2O_3 films by x-ray photoemission spectroscopy. They reported on the O_I peak for the first time, and attributed the splitting to the presence of additional O vacancies (V_O) in the structure. Their observed O_I-O_{II} energy separation of 1.5 eV is very close to our value. The double oxygen peak is characteristic of multiple valence cations. Ordinary O_{II}^{2-} ions occur with neighboring indium atoms having six O^{2-} neighbor ions. O_I^{2-} ions, on the other hand, occur in oxygen-deficient regions, and their neighboring In atoms have less than six O^{2-} neighbor ions. There is then also a possibly different charge density at the In^{3+} ions. It has been observed that the intensity and broadening of O_I^{2-} changes with O deficiency in studies of differently prepared thin films. The photon energy dependence in our study points also to an influence of the surface. The spectra at 640 eV are more surface sensitive than the 1000 eV spectra, which are closer to the ordinary laboratory Al- and Mg-K- α lines. This may be the reason why the weak In4d shoulders have been missed until now. It also points to a different electronic structure of bulk and surface V_O due to their different environment. We conclude that oxygen vacancies may play a role in In_2O_3 single crystals. Its role in doping has to be investigated further.

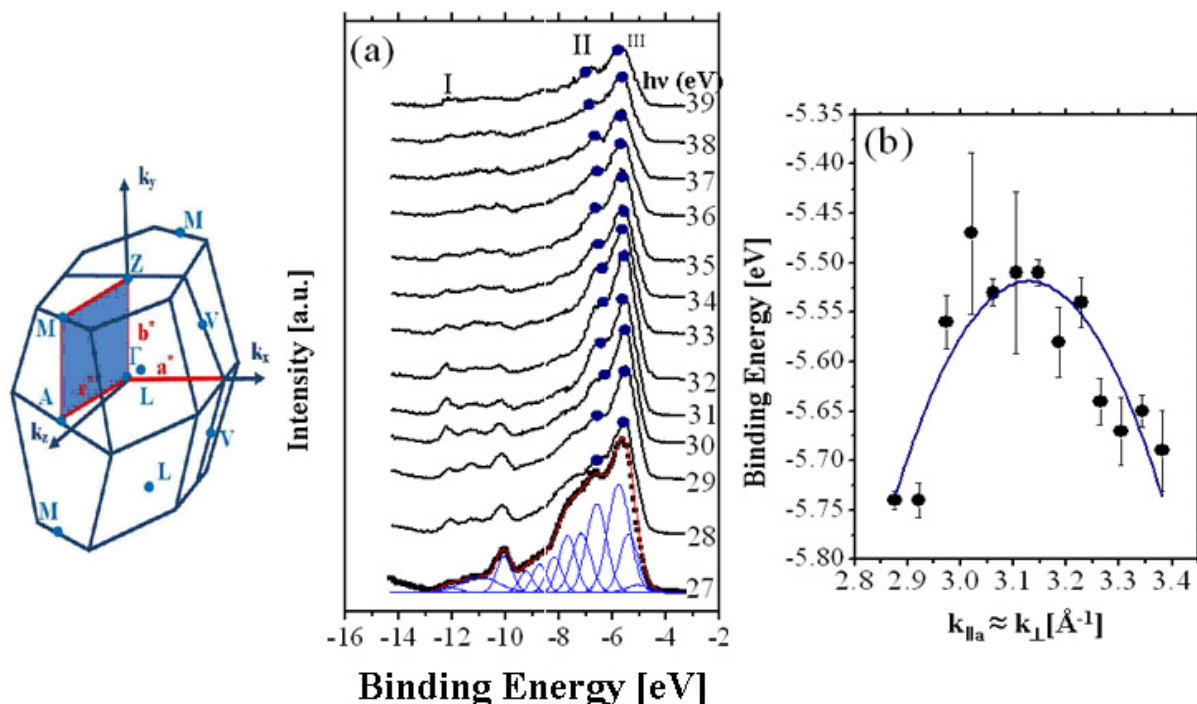


Figure 8. Left: BZ of Ga_2O_3 . The shape of the BZ of these base-centered monoclinic crystals depends strongly on the lattice parameters [14]. Since the cleavage plane is parallel to the b^* and c^* directions the normal emission spectra are not exactly along the high-symmetry line a^* . (a) Series of VB photoemission spectra normal to the b^*c^* -cleavage plane of the (100) surface of $\beta\text{-Ga}_2\text{O}_3$ single crystals at photon energies from 27 to 39 eV. (I), (II) and (III) label pronounced emission maxima (bands) near the bottom and the top of valence band. As an example, a fit of the VB by Gaussians after Shirley background subtraction is included in the 27 eV spectrum. (b) Dispersion of band (III) around 30 eV photon energy, i.e. around the Γ -point of the third BZ.

4. Ga_2O_3 : results and discussion

Ga_2O_3 has only 20 atoms per unit cell, greatly facilitating the observation of individual bands for comparison with theory. In this section we will therefore focus on a detailed comparison of experimental and theoretical band structures. Measurements made near normal emission along the a^* reciprocal line are depicted in figure 8(a). One observes a multitude of bands in figure 8(a), which we label in regions I, II and III. The bands of higher binding energies, included in region I, become very pronounced at photon energies around 30 eV. The two most prominent features, shown in regions II and III, were marked by solid dots. In figure 8(b) we show a symmetric experimental dispersion of the emission maximum III, which could be realized at an inner potential V_0 of 15 eV.

We have analyzed the dispersion of this strong emission feature III. We have not investigated the weak band at 4.9 eV binding energy that appears only in the shoulder of III. This weak state is due to the state forming the VBM (see the 27 eV spectrum of figure 8(a)). Since

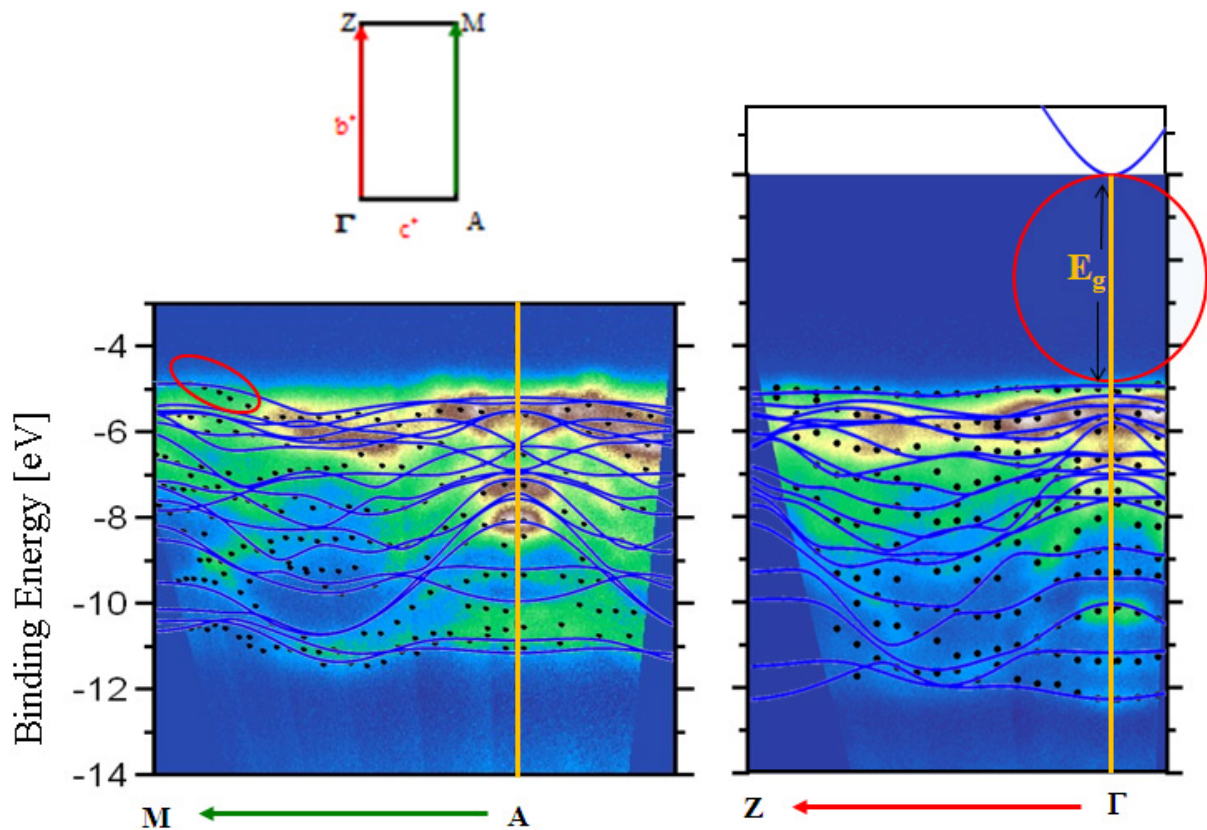


Figure 9. Top: BZ directions for Ga_2O_3 parallel to the cleavage plane (see also the previous figure). Bottom: experimental band structure of $\beta\text{-Ga}_2\text{O}_3$ along the A–M (left) and Γ –Z (b^*) (right) directions of the BZ. The experimental bands derived from a fitting procedure to the spectra are shown by black dots. Calculated band structures based on density functional theory using a hybrid functional are shown as blue lines on the experimental band structure for comparison. The red marked areas highlight the regions of the direct and indirect gaps.

in the a^* direction the separation of two Γ -points is 1.05 \AA^{-1} , the experimental curve shows the k_{\perp} -region around the Γ -point of the third BZ. A fit yielded effective masses of $0.28 \pm 0.01m_e$ for band III and $0.26 \pm 0.01m_e$ for band II. The total VB width is $7.37 \pm 0.02 \text{ eV}$ from the peak at -4.90 eV to the peak at -12.27 eV , respectively.

We now discuss two particular directions parallel to the cleavage face. Spectra were recorded at a photon energy of 30 eV to scan along the high-symmetry directions. Dispersion relations were obtained along the Γ –Z and A–M directions. They are depicted in figure 9 together with a theoretical band structure. At the Γ -point, bands at -12.27 , -11.50 and -10.00 eV show clear k -dispersion. Less intense bands appear below and above -9 eV . A manifold of bands between -4.9 and -8 eV appear as one wide band. The bands near the bottom of the VB at -12.27 and -10.00 eV merge at $0.5b^*$ in the b^* direction. The bands at a lower binding energy show only minor dispersion but high intensity, while the deeper-lying bands reveal more dispersion but are generally weaker. In the A–M direction at M, the width

of the valence bands is smaller than that at the Γ -point. In the A–M direction, the first band at higher binding energy is at -11.05 eV. The figure compares the experimentally determined bands from Γ to Z and from Γ to M with theoretical results based on density functional theory using a hybrid functional. Details of the calculations can be found in [15]. In the Γ –Z and Γ –M directions the band dispersions show excellent agreement with the calculated results. Along the Γ –M symmetry direction, one observes a maximum in the VB near the M-point and not at the Γ -point. This agrees with the theoretical calculations in [15] where, from theory, an indirect band gap with the VBM located slightly away from the M symmetry point and the CBM at the Γ -point was reported. The M-point states are only 50 meV above the states at Γ : E_g (direct) is 4.9 ± 0.1 eV, E_g (indirect) is 4.85 ± 0.1 eV and the VB width is 7.37 eV.

In a previous ARPES study on annealed surfaces of crystals grown by floating zone, only partial correspondence to theory was found [2]. In figure 9, from the Fermi energy down to -4.9 eV binding energy, no states appear in the energy gap. This was further checked by scanning this range for a long time without observing any intensity. This should not be surprising, as the doping level in Ga_2O_3 is two orders of magnitude lower than that of In_2O_3 . Since in n -type crystals the conduction band is located near E_F , the value of 4.9 eV represents within 100 meV the gap value, and is indeed close to the value of 4.8 eV [16] from optical measurements. Shallow donor levels in n -type Ga_2O_3 single crystals have recently been investigated experimentally [5] and theoretically [17].

5. Conclusions

Using ARPES and XPS we have determined the overall electronic VB structure of In_2O_3 single crystals and found three groups of bands, consistent with previous observations in thin films. The upper valence region (group III) and the lower-lying region composed of semicore In 4d-derived states (group I) are in good agreement with theoretical predictions [10, 11]. The VB states in between these two regions (group II), claimed by theory [10] to also be In 4d-derived, are in less satisfactory agreement with theory. The lower In_2O_3 conduction-band states were confirmed by XAS to be of O 2p character, and the higher conduction-band states to be of In 5p character. For Ga_2O_3 , a detailed comparison of bands determined by ARPES along major high-symmetry lines showed nearly perfect agreement with theory. Also the effective masses of Ga_2O_3 showed good agreement with theory. Furthermore, the experimental band gaps were determined by ARPES for both materials. For In_2O_3 , the band gap is direct and has the value 2.63 eV, but is forbidden in optical absorption. The states forming an optical band gap of $E_{g1} = 3.72$ eV could be identified. Also from ARPES, we find that the band gap of Ga_2O_3 is indirect and has the value $E_g = 4.85 \pm 0.1$ eV. Oxygen vacancies may play a role in In_2O_3 . By performing XPS at different photon energies, hints of a different electronic structure of bulk and surface oxygen vacancies in In_2O_3 were found.

Acknowledgments

This work is based on our study conducted at BESSY. We thank the staff of BESSY. This work was funded by DFG-NSF (under project numbers MA2371/8-1 and FO558/3-1) and the NSF MRSEC program (DMR05-20415). We also acknowledge the use of computing facilities at TeraGrid and TACC (NSF grant number DMR070072N). Mansour Mohamed thanks Mike Pietsch at the IKZ Berlin and the Ministry of Higher Education of Egypt and Assuit University for support.

References

- [1] Walsh A *et al* 2008 *Phys. Rev. Lett.* **100** 167402
- [2] Lovejoy T C, Yitamben E N, Shamir N, Morales J, Villora E G, Shimamura K, Zheng S, Ohuchi F S and Olmstead M A 2009 *Appl. Phys. Lett.* **94** 081906
- [3] King P D C, Veal T D, Payne D J, Bourlange A, Egdell R D and McConville C F 2008 *Phys. Rev. Lett.* **101** 116808
- [4] Schulz D, Ganschow S, Klimm D, Neubert M, Rossberg M and Schmidbauer M 2006 *J. Cryst. Growth* **296** 27
- [5] Galazka Z, Uecker R, Irmscher K, Albrecht M, Klimm D, Pietsch M, Brützm M, Bertram R, Ganschow S and Fornari R 2010 *Cryst. Res. Technol.* **45** 1229
- [6] Schmeißer D, Hoffmann P and Beuckert G 2005 *Materials for Information Technology, Devices, Interconnects and Packaging (Series: Engineering Materials and Processes)* (Berlin: Springer) ISBN 1-85233-941-1
- [7] J Åhman J, Svensson G and Albertsson 1996 *J. Acta Cryst. C* **52** 1336–8
- [8] Yamaga M, Villora E G, Shimamura K, Ichinose N and Honda M 2003 *Phys. Rev. B* **68** 155207
- [9] Weiher R L and Ley R P 1966 *J. Appl. Phys.* **37** 299
- [10] Karazhanov S Z, Ravindran P, Vajeeston P, Ulyashin A, Finstad T G and Fjellvåg H 2007 *Phys. Rev. B* **76** 075129
- [11] Fuchs F and Bechstedt 2008 *Phys. Rev. B* **77** 155107
- [12] Yeh J J 1993 *Atomic Calculation of Photoionization Cross Sections and Asymmetry Parameters* (London: Gordon and Breach)
- [13] Fan J C C and Goodenough J B 1977 *J. App. Phys.* **48** 3524
- [14] Ruzaiкин M P and Kudryavtseva N V 1974 *Russ. Phys. J.* **17** 934
- [15] Mohamed M, Janowitz C, Unger I, Manzke R, Galazka Z, Uecker R, Fornari R, Weber J R, Varley J B and Van de Walle C G 2010 *Appl. Phys. Lett.* **97** 211903
- [16] Orita M, Ohta H, Hirano M and Hosono H 2000 *Appl. Phys. Lett.* **77** 4166
- [17] Varley J B, Weber J R, Janotti A and Van de Walle C G 2010 *Appl. Phys. Lett.* **97** 142106